Vol 16 No 6, June 2007
1009-1963/2007/16(06)/1806-11
Chinese Physics
© 2007 Chin. Phys. Soc.
and IOP Publishing Ltd

Origination of gamma-ray burst pulses associated with the Doppler effect of spherical fireballs or uniform jet*

Lu Rui-Jing(陆睿静)[a], Qin Yi-Ping(覃一平)[a)b)c)], and Zhang Fu-Wen(张富文)[c)d)]

[a)] *Physical Science & Technology college, Guangxi University, Nanning* 530004, *China*
[b)] *Center for Astrophysics, Guangzhou University, Guangzhou* 510006, *China*
[c)] *National Astronomical Observatories/Yunnan Observatory, Chinese Academy of Sciences, Kunming* 650011, *China*
[d)] *The Graduate School of the Chinese Academy of Sciences, Beijing* 100049, *China*

(Received 4 March 2006; revised manuscript received 24 November 2006)

Ryde and Petrosian have pointed out that the rise phases of gamma-ray burst (GRB) pulses originate from the widths of the intrinsic pulses and their decay phases are determined by the curvature effect of the expanding fireball surface based on their simplified formula. In this paper we investigate in detail the issue based on the formula in Ref.[20], which is derived based on a model of highly symmetric expanding fireballs, where the Doppler effect is the key factor to be concerned about, and no terms are omitted in their derivation. Our analyses show that the decay phases of the observed pulses originate from the contributions from both the curvature effect of the expanding fireball and the two timescales of the local pulses, and the rise phases of the observed pulses only come from the two timescales of the local pulses. Associated with a local pulse with both rise and decay portions, the light curve of GRBs in the rise portion is expected to undergo a concave phase and then a convex one, whereas that in the decay portion is expected to evolve by an opposite process. And the ratio of the concave timescale to the convex one in the rise phase of the observed pulse linearly increases with the ratio of the rising timescale to the decay one of the local pulse ($r_{\rm rd}$), whereas the ratio of the convex timescale to the concave timescale in its decay phase linearly decreases with $r_{\rm rd}$. The two correlations are independent of the local pulse forms and the rest-frame radiation forms. But the different forms of local pulses and the different values of $r_{\rm rd}$ gives rise to the diversity of the light curve pulse shapes. We test a sample of 86 GRB pulses detected by the BATSE instrument on board the Compton Gamma Ray Observatory and find that the characteristics do exist in the light curve of GRBs.

Keywords: gamma-ray bursts, gamma-rays
PACC: 9580Q

1. Introduction

Light curves of gamma-ray bursts (GRBs) vary drastically in morphology, and no two GRBs are similar.[1] In the standard fireball model gamma rays are believed to result from shocks internal to the outflow at a distance of $R \sim 10^{13} - 10^{15}$ cm from the initial source.[2] A pulse in the gamma-ray light curve is generally considered to come from an individual shock episode. Superposition of many such pulses gives rise to the observed diversity and complexity of the light curves, which cannot be described by a simple formula. Although the most favoured GRB emission mechanisms are non-thermal synchrotron and/or inverse Compton emission.[3−6] some bursts are found to have thermal spectra during the initial phase before they become non-thermal emission.[7−11] Therefore, the spectral and temporal characteristics hold the keys of a good understanding of the prompt emission of GRBs.

In spite of the very complex temporal behaviour of the GRBs, many attempts have been made to decompose the complex light curves into pulses, which can be described by several flexible functions based on empirical or semi-empirical relations, and quantify their characteristics.[12−17] These well-separated pulses appear as asymmetric profiles with a fast rise and an exponential decay (FRED).[12,18,19] And some relations can be found from the investigations of GRBs with the simple FRED pulses.

However, what physical mechanism(s) causes such an observed pulse? In the Fenimore *et al*'s model,[13] the rise phase of a FRED pulse is considered to result from the duration of the photon-active phase and its fall phase is related to the duration of the photon-quiet phase. But in Ryde and Petrosian's model,[17]

*Project supported by the National Natural Science Foundation of China (Grant No 10463001) and the Research Foundation of Guangxi University (Grant No DD052018).

the rise phases of the observed pulses come from the dynamic time, which is consistent with the fact that the rise phase is produced by the width of a local pulse in Ref.[20], (note that here the width of the intrinsic pulse is referred to as the dynamic time); and the decay phases of the observed pulses are determined by the curvature effect of the expanding fireball surface. And a similar conclusion has also been found by Shen *et al.*[21] However, we want to know what role the rise and decay phases of local pulses (or intrinsic pulses) each play in the observed light curve of the gamma-ray burst, and what is responsible for the diversity of the FRED pulses. Motivated by these, we explore in this paper possible explanations for the pulse shapes observed based on Qin *et al*'s model.[20]

According to the observed output rate of radiation, the observed gamma-ray pulses are believed to be produced from a highly relativistic outflow, (e.g. an expanding and collimated fireball), based on the large energies and the short timescales involved. In the case of a spherical fireball, the Doppler effect over the whole fireball must do its work, and the observed FRED structure probably provides the intrinsical information. Qin[22] has derived the flux function based on the model of highly symmetric expanding fireball, where the Doppler effect of the expanding fireball surface is a key factor to be concerned about, and then with this formula, Qin[23] has further studied how this effect exerts an influence on the emission and absorbtion lines. Recently, Qin *et al*[20] have presented the formula in terms of count rates, which can also be applicable to the case of a uniform jet as long as the open angle of the jet is taken into account. This model leads to the unveiling of certain relations, such as a power law relationship between the observed pulse width and energy,[24] an anti-correlation between the power law index and the local pulse width,[25] and a linear correlation between the observed pulse and the local pulse width,[26] but there is no significant correlation between the ratio of the full width at half maximum (FWHM) width of the rise phase of the observed pulse to that of the decay phase and the Lorentz factor,[27] and correlations between spectral lags and such physical parameters as the Lorentz factor and the fireball radius.[28] Combining the characteristics described above and a reverse S-feature in the decay phase of the observed pulse,[29] we suspect that the curvature effect of the expanding fireball and the local pulse can make different contributions to the observed pulse profile.

This paper is organized as follows. In Section 2, we present the characteristics of the light curve of GRBs obtained from our theoretical analysis based on a uniform jet and a spherical fireball model. In Section 3, we examine the characteristics of the light curves of a GRB sample detected by the BATSE instrument on board the Compton Gamma Ray Observatory. Discussion and conclusions are presented in the last section.

2. Numerical analysis

As derived in detail by Qin *et al*,[20] the expected count rate of the fireball within frequency interval $[\nu_1, \nu_2]$ can be calculated with their equation (21), which is rewritten as follows:

$$C(\tau) = \frac{2\pi R_c^3 \int_{\tilde{\tau}_{\theta,\min}}^{\tilde{\tau}_{\theta,\max}} \widetilde{I}(\tau_\theta)(1+\beta\tau_\theta)^2(1-\tau+\tau_\theta)\mathrm{d}\tau_\theta \int_{\nu_1}^{\nu_2} \frac{g_{0,\nu}(\nu_{0,\theta})}{\nu}\mathrm{d}\nu}{hcD^2\Gamma^3(1-\beta)^2(1+k\tau)^2}. \quad (1)$$

In this formula, τ_θ is a dimensionless relative local time defined by $\tau_\theta \equiv c(t_\theta - t_\mathrm{c})/R_\mathrm{c}$, where t_θ is the emission time in the observer frame, called local time, of photons emitted from the concerned differential surface $\mathrm{d}s_\theta$ of the fireball (θ is the angle to the line of sight), t_c is a constant which can be assigned to any value of t_θ, and R_c is the radius of the fireball measured at $t_\theta = t_\mathrm{c}$; variable τ is a dimensionless relative time defined by $\tau \equiv [c(t-t_\mathrm{c}) - D + R_\mathrm{c}]/R_\mathrm{c}$, where D is the distance of the fireball to the observer, and t is the observation time; $\widetilde{I}(\tau_\theta)$ represents the development of the intensity magnitude in the observer frame, called a local pulse function; $g_{0,\nu}(\nu_{0,\theta})$ describes the rest frame radiation mechanisms; And $k \equiv \beta/(1-\beta)$. At the same time, the integral lower and upper limits, $\tilde{\tau}_{\theta,\min}$ and $\tilde{\tau}_{\theta,\max}$, are determined by $\tilde{\tau}_{\theta,\min} = \max\{\tau_{\theta,\min}, (\tau - 1 + \cos\theta_{\max})/(1 - \beta\cos\theta_{\max})\}$ and $\tilde{\tau}_{\theta,\max} = \min\{\tau_{\theta,\max}, (\tau - 1 + \cos\theta_{\min})/(1 -$

$\beta\cos\theta_{\min})\}$, respectively, where $\tau_{\theta,\min}$ and $\tau_{\theta,\max}$ are the lower and upper limits of τ_θ confining $\widetilde{I}(\tau_\theta)$, and $\theta_{\min}$ and $\theta_{\max}$ are confined by the emitting surface of the fireball, and then the radiation is observable within the range of $(1-\cos\theta_{\min})+(1-\beta\cos\theta_{\min})\tau_{\theta,\min} \le \tau \le (1-\cos\theta_{\max})+(1-\beta\cos\theta_{\max})\tau_{\theta,\max}$.

2.1. In the case of radiation emitted from the whole fireball surface

If the radiation is emitted from the whole fireball surface, we can take $\theta_{\min}=0$ and $\theta_{\max}=\pi/2$. Therefore the range of τ is $(1-\beta)\tau_{\theta,\min} \le \tau \le 1+\tau_{\theta,\max}$, while $\tilde{\tau}_{\theta,\min}$ and $\tilde{\tau}_{\theta,\max}$ are determined by

$$\tilde{\tau}_{\theta,\min} = \max\{\tau_{\theta,\min}, \tau-1\}$$

and $\tilde{\tau}_{\theta,\max} = \min\{\tau_{\theta,\max}, \tau/(1-\beta)\}$, respectively.

Formula (1) suggests that, except for the state parameters of the fireball (i.e. Γ, $R_{\rm c}$ and D), the light curves of sources depend on $\tilde{I}(\tau_\theta)$ and $g_{0,\nu}(\nu_{0,\theta})$. Observations suggest that the common radiation form of GRBs is the so-called Band function[30] which is frequently and rather successfully employed to fit the spectra of the sources.[31−35] Combining with the fact that the observed radiation form is only be affected slightly by the fireball Doppler effect,[22] we suspect that the rest frame radiation of many fireball sources may bear the same forms as those in the observer frame. Therefore, we assume in this paper the band function to be an intrinsic mechanism, and its form can be written as

$$g_{0,\nu}(\nu_{0,\theta}) = \begin{cases} \left(\frac{\nu_{0,\theta}}{\nu_{0,p}}\right)^{1+\alpha_0}\exp\left[-(2+\alpha_0)\frac{\nu_{0,\theta}}{\nu_{0,p}}\right], & \left(\frac{\nu_{0,\theta}}{\nu_{0,p}} < \frac{\alpha_0-\beta_0}{2+\alpha_0}\right), \\ \left(\frac{\alpha_0-\beta_0}{2+\alpha_0}\right)^{\alpha_0-\beta_0}\exp(\beta_0-\alpha_0)\left(\frac{\nu_{0,\theta}}{\nu_{0,p}}\right)^{1+\beta_0}, & \left(\frac{\nu_{0,\theta}}{\nu_{0,p}} \ge \frac{\alpha_0-\beta_0}{2+\alpha_0}\right), \end{cases} \tag{2}$$

where α_0 and β_0 are the low- and high-energy indices in the rest frame, respectively, and $\nu_{0,p}$ is the rest-frame peak frequency. According to the Doppler effect, the observed frequency (ν) is related to the rest frame frequency ($\nu_{0,\theta}$) by $\nu_{0,\theta} = (1-\beta+\beta\tau)\Gamma\nu/(1+\beta\tau_\theta)$.

We pay our attention to the roles that the rise and decay portions of local pulses play in the light curve of gamma-ray bursts. For simplicity, a local pulse with a power law rise and a power law decay is first employed to study in detail this issue, which is written as

$$\widetilde{I}(\tau_\theta) = I_0 \begin{cases} \left(\frac{\tau_\theta-\tau_{\theta,\min}}{\tau_{\theta,0}-\tau_{\theta,\min}}\right)^{\mu}, & (\tau_{\theta,\min} \le \tau_\theta \le \tau_{\theta,0}), \\ \left(1-\frac{\tau_\theta-\tau_{\theta,0}}{\tau_{\theta,\max}-\tau_{\theta,0}}\right)^{\mu}, & (\tau_{\theta,0} < \tau_\theta \le \tau_{\theta,\max}), \end{cases} \tag{3}$$

where I_0, μ and $\tau_{\theta,0}$ are constants. We notice that the width of the local pulse, $\Delta\tau_{\theta,\rm FWHM} = (1-2^{-1/\mu})(\tau_{\theta,\max}-\tau_{\theta,\min})$ and therefore its upper limit, $\tau_{\theta,\max} = \Delta\tau_{\theta,\rm FWHM}/(1-2^{-1/\mu})+\tau_{\theta,\min}$. For a given value of $\tau_{\theta,\max}$, the rise width, $\Delta\tau_{\theta,r}$, and the decay width, $\Delta\tau_{\theta,d}$, of the local pulse vary with the value of $\tau_{\theta,0}$. We thus assign

$$\tau_{\theta,0} = \tau_{\theta,\min} + e(\tau_{\theta,\max}-\tau_{\theta,\min}), \tag{4}$$

where the quantity, e, is a constant within the range of $0 \le e \le 1$. We define that $\Delta\tau_{\theta,r} = \tau_{\theta,0}-\tau_{\theta,\min}$, $\Delta\tau_{\theta,d} = \tau_{\theta,\max}-\tau_{\theta,0}$, and

$$r_{\rm rd}(e) = \frac{\Delta\tau_{\theta,r}}{\Delta\tau_{\theta,d}}, \tag{5}$$

the quantity $r_{\rm rd}(e)$ denotes the ratio of the rise timescale to the decay timescale of a local pulse.

To describe different contributions of $\Delta\tau_{\theta,r}$ and $\Delta\tau_{\theta,d}$ of a local pulse to the light curve, we define

$$C_{\rm r}(\tau) = \frac{2\pi R_{\rm c}^3 \int_{\tilde{\tau}_{\theta,\min}}^{\tilde{\tau}_{\theta,\max}} \widetilde{I}(\tau_\theta)(1+\beta\tau_\theta)^2(1-\tau+\tau_\theta)\mathrm{d}\tau_\theta \int_{\nu_1}^{\nu_2} \frac{g_{0,\nu}(\nu_{0,\theta})}{\nu}\mathrm{d}\nu}{hcD^2\Gamma^3(1-\beta)^2(1+k\tau)^2}, \qquad (\tau_{\theta,\min} \le \tau_\theta \le \tau_{\theta,0}), \tag{6}$$

$$C_{\rm d}(\tau)=\frac{2\pi R_{\rm c}^3\int_{\tilde{\tau}_{\theta,\min}}^{\tilde{\tau}_{\theta,\max}}\widetilde{I}(\tau_\theta)(1+\beta\tau_\theta)^2(1-\tau+\tau_\theta){\rm d}\tau_\theta\int_{\nu_1}^{\nu_2}\frac{g_{0,\nu}(\nu_{0,\theta})}{\nu}{\rm d}\nu}{hcD^2\Gamma^3(1-\beta)^2(1+k\tau)^2},\qquad(\tau_{\theta,0}<\tau_\theta\leq\tau_{\theta,\max}),\tag{7}$$

$$r_{\rm r}=\frac{C_{\rm r}(\tau)}{C(\tau)},\tag{8}$$

and

$$r_{\rm d}=\frac{C_{\rm d}(\tau)}{C(\tau)},\tag{9}$$

where $C(\tau)=C_{\rm r}(\tau)+C_{\rm d}(\tau)$. Quantities $C_{\rm r}(\tau)$ and $C_{\rm d}(\tau)$ denote the contributions of the rise timescale and decay timescale of a local pulse to the light curve, respectively.

Let us first employ Eq.(3) with $\mu=1$ (note that when $\mu=1$, the local pulse (3) becomes a linear rise and a linear decay one), and the Band function radiation form with $\alpha_0=-1$, $\beta_0=-2.25$ and $\nu_{0,p}=1$ keVh^{-1} within the frequency range of 100 keVh$^{-1}\leq\nu\leq$ 300 keVh^{-1} to make light curves. In order to obtain more detailed information of the light curve profiles, we evaluate the first-order derivatives, $C'_{\rm r}(\tau)$, $C'_{\rm d}(\tau)$, $C'(\tau)$, and the second-order derivatives $C''_{\rm r}(\tau)$, $C''_{\rm d}(\tau)$, $C''(\tau)$, of the count rate $C_{\rm r}(\tau)$, $C_{\rm d}(\tau)$, $C(\tau)$, respectively. Their profiles are presented in Fig.1.

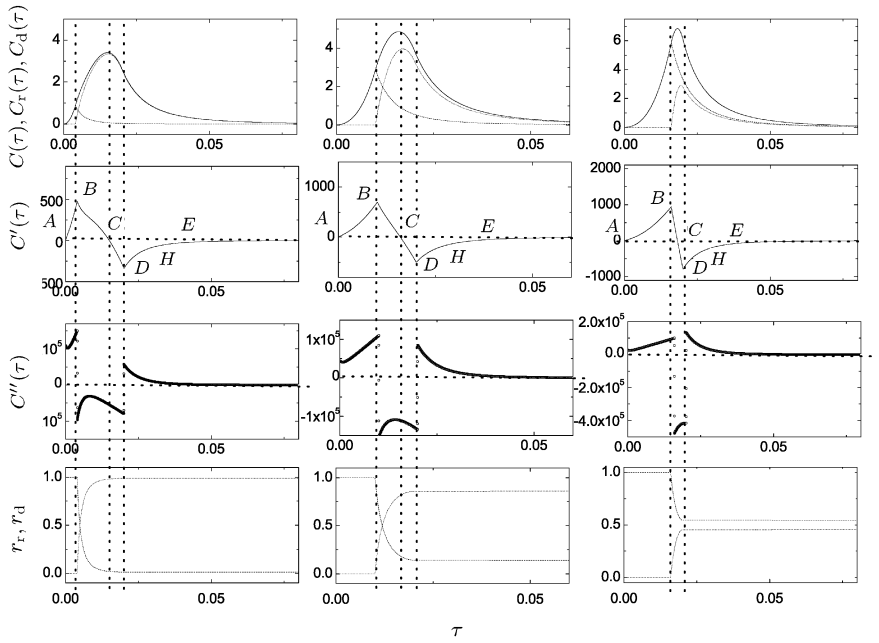


Fig.1. Plots of $C(\tau)$, $C_{\rm r}(\tau)$, $C_{\rm d}(\tau)-\tau$ (the first row), $C'_{\rm r}(\tau)-\tau$ (the second row), $C''_{\rm r}(\tau)-\tau$ (the third row), $r_{\rm r}/r_{\rm d}-\tau$ (the last row), of the light curves associated with a local pulse determined by Eq.(3). A Band function is adopted as a rest frame radiation form, where $\alpha_0=-1$, $\beta_0=-2.25$ and $\nu_{0,p}=1$ keVh^{-1}. In addition, we take $2\pi R_{\rm c}^3 I_0/hcD^2=1$, Γ=100, μ=1, $\Delta\tau_{\theta,\rm FWHM}=2$, 100 keVh$^{-1}\leq\nu\leq$ 300 keVh^{-1} and $\tau_{\theta,\min}=0$, $e=0.2, 0.5, 0.8$ (from left to right) respectively. The solid, dashed and dotted lines in the first row represent $C(\tau)$, $C_{\rm r}(\tau)$, $C_{\rm d}(\tau)$, respectively. The dashed and dotted lines in the last row denote $r_{\rm r}$ and $r_{\rm d}$, respectively.

As shown in Fig.1, there is an inflexion from concavity to convexity in the rise phase of the light curve: two phases, $A-B$ and $D-E$, undergo a concave process as $C''_{AB}(\tau)>0$ and $C''_{DE}(\tau)>0$, whereas other two phases, $B-C$ and $C-D$, evolve a convex phase because of $C''_{BC}(\tau)<0$ and $C''_{CD}(\tau)<0$. We also find from the figure that both the rise timescale and the decay one of the local pulse make contributions to the two portions of the light curves. The rise portion of the local pulse produces concave phases on both sides of the light curve and creates a spiky profile, whereas the decay one yields a convex phase in the rising portion, and a convex-to-concave phase in the decay portion of the light curve, and gives birth to a smooth profile. In other words, the joint contributions of both portions of the local pulse lead to the light curve with its rising portion to evolve from a concave phase to a convex one (the so-called 'concave-to-convex' character), and that with its decay portion undergoes an opposite process (the so-called 'convex-to-concave' one),

which may be the reason why a reverse S-feature curve generally exists in the decay phase of the observed pulse.[29] Therefore, a local pulse with a small value of $r_{\rm rd}$ can produce a flat-topped light curve, which is corresponding to a large value of ν in Norris *et al*'s[12] model (note that ν is a measure of pulse sharpness in their paper), whereas a local pulse with a large value of $r_{\rm rd}$ yields a spiky light curve, which corresponds to a small value of ν.

We define

$$r_{\rm cv1} = \frac{\tau_{AB}}{\tau_{BC}} \tag{10}$$

and

$$r_{\rm cv2} = \frac{\tau_{CD}}{\tau_{DH}} \tag{11}$$

to denote the ratio of the two time intervals from concavity to convexity in the rise portion of the light curve, and that from convexity to concavity in the decay portion, respectively, where H denotes the point at the half-maximum position of the $D-E$ phase, and subscripts 'c' and 'v' represent concavity and convexity respectively. The relationships between $r_{\rm cv1}$ and $r_{\rm rd}$, and between $r_{\rm cv2}$ and $r_{\rm rd}$ are plotted in Fig.2 (see the solid lines in the figure).

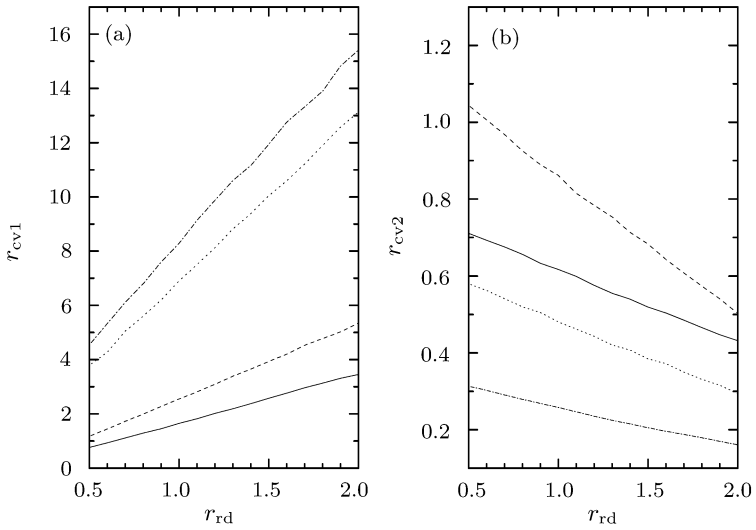


Fig.2. Relationships between $r_{\rm cv1}$ and $r_{\rm rd}$, and between $r_{\rm cv2}$ and $r_{\rm rd}$ in the light curve pulses Eq.(1) associated with the local power law pulses Eq.(3) with $\mu = 1$ (solid lines), 2 (dash lines), local exponential pulse Eq.(12) (dot lines) and local Gaussian pulse Eq.(13) (dash dot lines). We take $\sigma_1 + \sigma_2 = 2$. Other parameters are the same as those adopted in Fig.1.

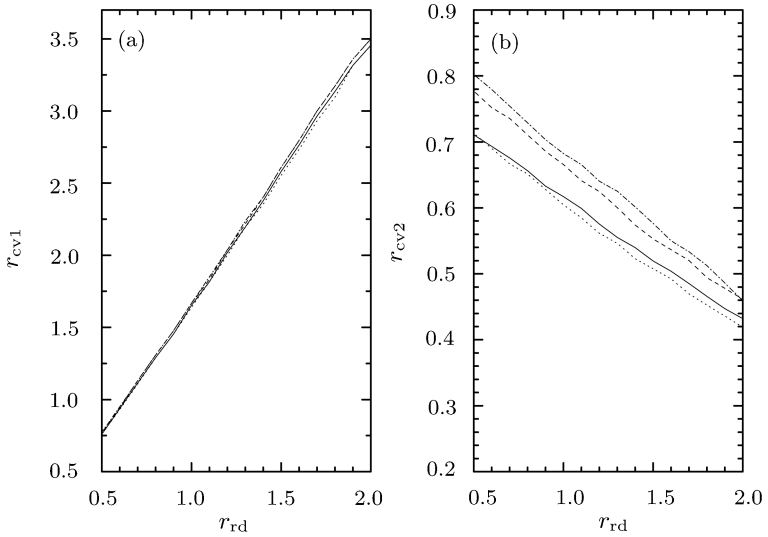


Fig.3. Relationships between $r_{\rm cv1}$ and $r_{\rm rd}$, and between $r_{\rm cv2}$ and $r_{\rm rd}$ in the light curve pulses Eq.(1) associated with the local power law pulse Eq.(3) with $\mu = 1$ for the rest frame spectral indices of $(\alpha_0, \beta_0) = (-1, -2.25)$ (the solid lines), $(-1, -4.5)$ (the dashed lines), $(-0.5, -2.25)$ (the dot lines) and $(-0.5, -4.5)$ (the dash-dotted lines). Other parameters are the same as those adopted in Fig.1.

We find from Fig.2 that $r_{\rm cv1}$ increases linearly with $r_{\rm rd}$ for the light curve associated with the local pulse defined by Eq.(3) with $\mu = 1$, while $r_{\rm cv2}$ decreases linearly with $r_{\rm rd}$. When performing linear least square fit to the two quantities, we have $r_{\rm cv1} = (-0.111 \pm 0.014) + (1.787 \pm 0.012) r_{\rm rd}$ and $r_{\rm cv2} = (0.808 \pm 0.003) - (0.191 \pm 0.001) r_{\rm rd}$.

With the local pulse widths being different, such as $\Delta\tau_{\theta,\rm FWHM}$ ranging from 0.2 to 20, we find that the two relevant curves are not significantly changed.

One might ask what situations can happen if the rest frame spectrum varies with time. Figures 3 and 4 illustrate the influences of the rest frame radiation forms on the two relationships. One can find from the two figures that the relationship between $r_{\rm cv1}$ and $r_{\rm rd}$ is less affected by the rest frame spectral indices, but largely affected by the rest frame spectral hardness; and the relationship between $r_{\rm cv2}$ and $r_{\rm rd}$ is somewhat affected by both the rest frame spectral hardness and indices: the larger the value of the spectral hardness, the more obvious the effect.

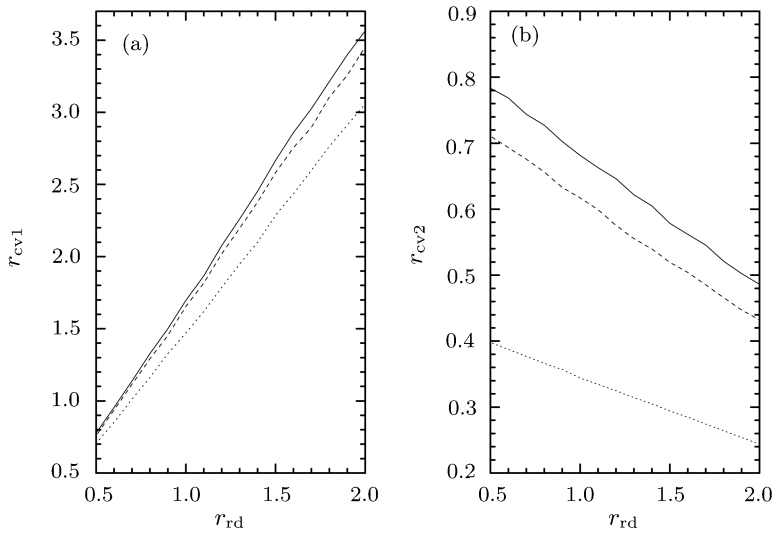


Fig.4. Relationships between $r_{\rm cv1}$ and $r_{\rm rd}$, and between $r_{\rm cv2}$ and $r_{\rm rd}$ in the light curve pulses Eq.(1) associated with the local power law pulse Eq.(3) with $\mu = 1$ for the rest frame spectral hardness of $\nu_{0,p} = 0.1$ keVh^{-1} (the solid lines), 1 keVh^{-1} (the dashed lines), 10 keVh^{-1} (the dotted lines). Other parameters are the same as those adopted in Fig.1.

To check whether the local pulse form depends on the profile of light curve, besides the local pulse determined by Eq.(3) with $\mu = 2$, we also consider three other local pulse forms. The first pulse is a local pulse with an exponential rise and an exponential decay phases

$$\widetilde{I}(\tau_\theta) = I_0 \begin{cases} \exp\Big(\dfrac{\tau_\theta - \tau_{\theta,0}}{\sigma_1}\Big), & (\tau_{\theta,\rm min} \le \tau_\theta \le \tau_{\theta,0}), \\ \exp\Big(-\dfrac{\tau_\theta - \tau_{\theta,0}}{\sigma_2}\Big), & (\tau_{\theta,0} < \tau_\theta), \end{cases} \tag{12}$$

The second pulse is in a local Gaussian form

$$\widetilde{I}(\tau_\theta) = I_0 \begin{cases} \exp\Big[-\Big(\dfrac{\tau_\theta - \tau_{\theta,0}}{\sigma_1}\Big)^2\Big], & (\tau_{\theta,\rm min} \le \tau_\theta \le \tau_{\theta,0}), \\ \exp\Big[-\Big(\dfrac{\tau_\theta - \tau_{\theta,0}}{\sigma_2}\Big)^2\Big], & (\tau_{\theta,0} < \tau_\theta). \end{cases} \tag{13}$$

The third pulse is of a local δ-function

$$\widetilde{I}(\tau_\theta) = \frac{cI_0}{R_{\rm c}} \delta(\tau_\theta - \tau_{\theta,0}), \qquad (\tau_{\theta,\rm min} \le \tau_\theta \le \tau_{\theta,\rm max}). \tag{14}$$

A study shows that the conclusions obtained above hold for all these local pulses except the pulse in the form of local δ-function. The difference stems from the dependence of local pulse form on slope (see the $r_{\rm cv}$ and $r_{\rm rd}$ panels and also see Fig.2). We thus perform linear least square fit at 1σ confidence level to the two quantities, and have $r_{\rm cv1} = (-0.167\pm0.014)+(2.735\pm0.012)r_{\rm rd}$ and $r_{\rm cv2} = (1.225\pm0.002)-(0.363\pm0.002)r_{\rm rd}$ for the local pulse determined by Eq.(3) with $\mu = 2$, $r_{\rm cv1} = (0.534 \pm 0.025) + (6.318 \pm 0.021)r_{\rm rd}$ and $r_{\rm cv2} = (0.674 \pm 0.001) - (0.191 \pm 0.001)r_{\rm rd}$ for the local pulse determined by Eq.(12), and $r_{\rm cv1} = (0.695\pm0.089)+(7.483\pm0.074)r_{\rm rd}$ and $r_{\rm cv2} = (0.365\pm0.001) - (0.105 \pm 0.001)r_{\rm rd}$ for the local pulse determined by Eq.(13). For all these situations of fitting, their linear correlation coefficients $R > 0.999$, and their probabilities $p < 10^{-4}$.

Associated with a local δ-function pulse, the profile of the light curve can be found in Fig.1 in Ref.[3]. There is no rise phase in the light curve for neither rise nor decay timescale in the local δ-pulse. But there is a decay phase which also undergoes a convex-to-concave profile variation. Combining the information above, we find that, as pointed out in some literature,[17,28] the rise phases of light curves are always dominated by the emission at $\theta \simeq 0$, the rise phase of the light curve only comes from the contributions from the rise and decay timescales of a local (or intrinsic) pulse, but the decay phase of the light curve results not only from the contributions of the two timescales, but also from that of the curvature effect of the expanding fireball.

2.2. In the case of radiation emitted from a uniform jet

If the radiation is emitted from a jet-like geometry with a half-opening angle θ_j and a spherical surface (a uniform jet), we assume that for such a relativistic outflow both the Lorentz factor Γ and the energy per unit solid angle from the jet axis are constant during the GRB phase, and that the observer direction is along the jet axis. Under these assumptions, we can apply Eq.(1) to the uniform jet by taking $\theta_{\rm min} = 0$ and $\theta_{\rm max} = \theta$, where θ represents the half-opening angle of the jet.

With $\Gamma = 10$ or 100, $\theta_{\rm min} = 0$ and $\theta_{\rm max} = \Gamma^{-1}$, we repeat the same work as done in Section 2.1, and find the same conclusions as the above, except for a cutoff tail feature appearing in the decay portion (see Fig.1 in Ref.[20]). (The cutoff tail feature does not appear in a light curve when $\theta_{\rm max} \gg \Gamma^{-1}$ or the corresponding local pulse width becomes large enough such that $\Delta\tau_{\theta,\rm FWHM} \geq 1$). The characteristics of light curves appear to result from the Doppler effect of a spherical fireball or a uniform jet as long as its radiation-emitting surface is spherical.

3. Observational data

Motivated by whether or not the characteristic, a 'concave-to-convex' phase in the rise portion of light curve pulse and its decay portion undergoing an opposite process, indeed exists in the observed light curves, we investigate the profiles of light curves of GRBs detected by the BATSE instrument on board the CGRO (Compton Gamma Ray Observatory). It is already known that pulses of a GRB have a tendency of self-similarity for different energy bands.[12] Therefore we study in this paper the issue based only on the count rate of the 3rd channel.

For each source, the background is estimated by a fit with a polynomial expression using 1.024s resolution data that are available from ten minutes before the trigger to several minutes after the burst. The data along with the background fit coefficients can be obtained from the public archives of CGRO Science Support Center (CGROSSC) at NASA Goddard Space Flight Center. We smooth the background-subtracting light curves with the DB3 wavelet with the MATLAB software in the level of the third-class decomposition. The selections from these data give rise to a sample comprising 86 well-separated pulses, on which almost no other small pulses overlap.

When evaluating the first-order derivative, $C'(t)$, for each pulse in our sample, we find that the characteristic mentioned above generally exists in our sample. We obtain the values of $r_{\rm cv1}$ and $r_{\rm cv2}$ in an observed pulse by identifying the characteristic points of B, C and D in the $C'(t)$ curve and the characteristic points of A and H in the corresponding observed pulse. Applying this method, we obtain the values of $r_{\rm cv1}$ and $r_{\rm cv2}$ for our sample pulses as shown in Table 1. The distributions of $r_{\rm cv1}$ and $r_{\rm cv2}$ are presented in Fig.5.

Figure 5 shows that there exist different values of $r_{\rm cv1}$ and $r_{\rm cv2}$ in our sample, with $r_{\rm cv1}$ ranging from 0.11 to 11.29 and its mean value being 2.41 and with $r_{\rm cv2}$ varying from 0.17 to 0.93 and its mean value being 0.56, indicating that, according to the above theoretical analysis, these observed pulses may result either

from the local pulses with different values of $r_{\rm rd}$ or from different local pulse forms, or from both. The observed distributions of $r_{\rm cv1}$ and $r_{\rm cv2}$, for which the explanation is not clear, may constrain the mechanism(s) of the birth of local pulses.

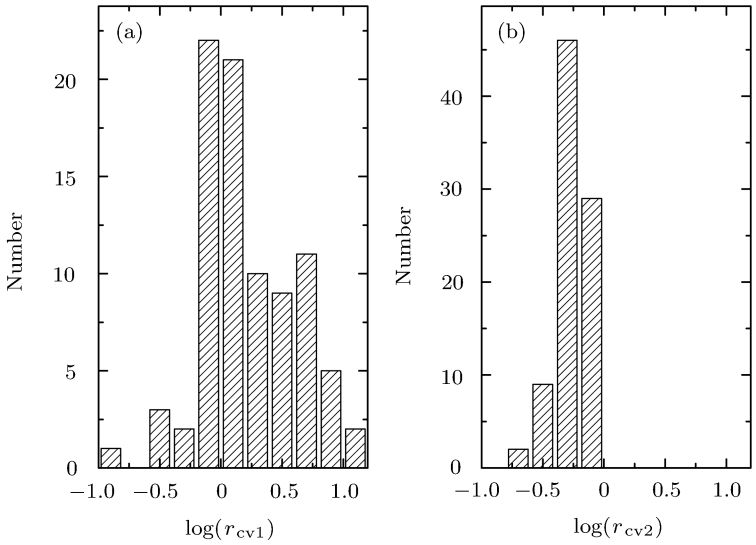


Fig.5. Distributions of $r_{\rm cv1}$ and $r_{\rm cv2}$ of all pulses in our sample.

Figure 6 illustrates the light curves and their slopes of three typical events with different values of ($r_{\rm cv1}$, $r_{\rm cv2}$) = (0.42, 086) for ♯ 07374, (1.69, 0.41) for ♯ 01883 and (5.01, 0.56) for ♯ 01733. Note that for the sake of comparison, the selected pulses are normalized and their variable, t, is re-scaled such that the peak count rate is located at $t' = 0$ and the FWHM point of the decay portion is located at $t' = 0.2$.

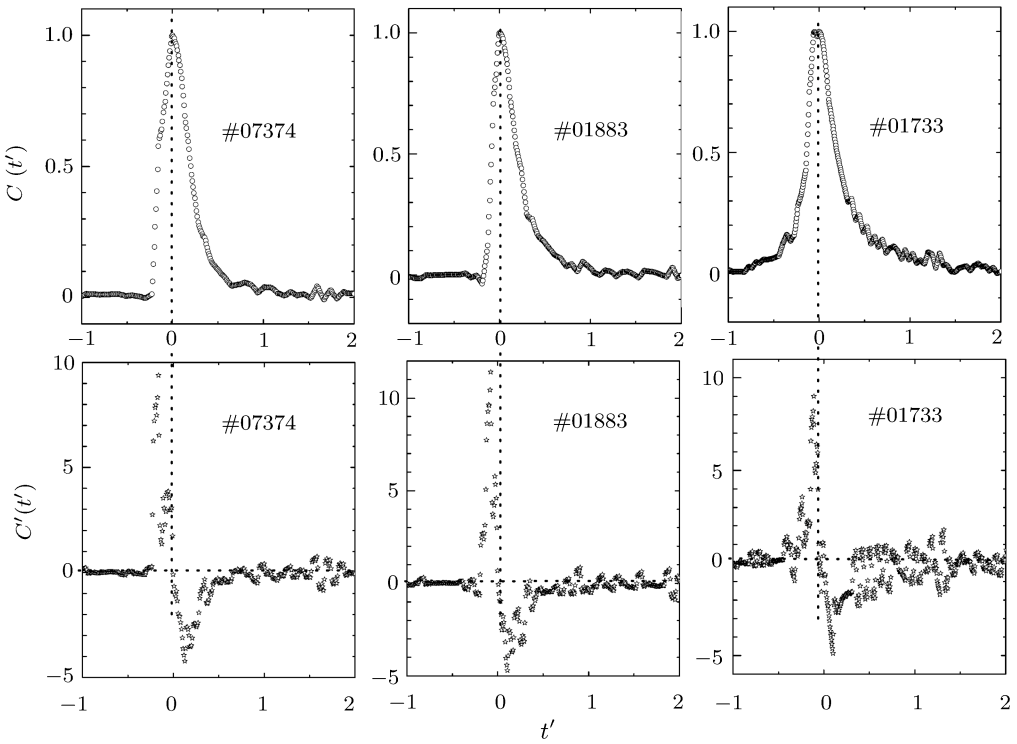


Fig.6. Illustration of the observed pulses (first row) and their slopes (second row) for three typical events selected from our sample.

Table 1. The values of r_{cv1} and r_{cv2} for our sample pulses.

trigger number	r_{cv1}	r_{cv2}	trigger number	r_{cv1}	r_{cv2}	trigger number	r_{cv1}	r_{cv2}
493	0.70	0.59	2665	0.80	0.83	5474	1.15	0.89
563	0.91	0.29	2700	3.53	0.63	5478	0.50	0.53
829	0.96	0.39	2749	11.29	0.69	5495	0.93	0.70
907	0.69	0.66	2880	7.85	0.69	5517	1.70	0.54
914	2.05	0.65	2919	1.48	0.58	5523	7.47	0.27
973	0.99	0.68	3040	1.31	0.41	5601	1.02	0.66
973	0.80	0.59	3143	6.19	0.51	5601	1.52	0.61
999	4.17	0.17	3155	0.76	0.77	6225	0.31	0.36
1157	7.75	0.17	3256	1.63	0.30	6335	2.84	0.55
1406	0.69	0.51	3237	1.44	0.49	6397	1.02	0.42
1467	2.71	0.48	3257	1.23	0.93	6504	0.70	0.52
1700	1.11	0.67	3415	0.66	0.75	6621	2.00	0.63
1733	5.01	0.56	3648	3.58	0.46	6672	1.26	0.40
1883	1.69	0.41	3668	2.87	0.49	6672	0.82	0.43
1956	1.56	0.76	3765	1.92	0.41	6930	1.70	0.55
1989	0.11	0.48	3866	4.20	0.55	7293	1.46	0.91
2083	4.68	0.46	3870	1.29	0.62	7295	1.51	0.59
2102	2.41	0.36	3875	0.63	0.46	7374	0.42	0.86
2138	1.99	0.78	3886	4.50	0.50	7403	0.65	0.74
2267	4.52	0.54	3892	0.85	0.49	7548	1.18	0.47
2306	4.90	0.33	3954	7.85	0.37	7548	0.70	0.93
2387	0.70	0.77	4157	1.36	0.36	7588	0.90	0.65
2393	7.28	0.50	4350	0.90	0.54	7638	3.80	0.39
2393	2.99	0.58	4350	2.75	0.60	7648	1.45	0.66
2431	6.05	0.50	4350	2.52	0.49	7701	4.72	0.50
2484	1.12	0.86	4368	1.02	0.67	7711	0.38	0.62
2519	4.07	0.84	4368	0.74	0.43	7744	10.74	0.30
2530	0.37	0.50	4710	0.89	0.73	8111	2.40	0.64
2662	1.19	0.52	5415	1.39	0.42			

4. Discussion and conclusions

All analyses in this paper are based on formula (1), which is suitable for describing the light curves of the spherical fireballs or the uniform jets. Numerical calculations show that the characteristics, the 'concave-to-convex' phase in the rise portion and the 'convex-to-concave' phase in the decay portion, and the values of r_{cv1} and r_{cv2} of light curves, are not affected by the Lorentz factor Γ and the half-opening angle θ_j.

Besides the Band function spectrum, the Comptonized spectrum and the broken power-law spectrum have been employed to fit the spectral data.[34,35] Therefore, we also employ the two spectra as the rest-frame radiation forms to investigate the influence of the rest frame radiation forms on a light curve profile and find that the characteristics of the resultant light curve profile do hold for these rest-frame forms and the different rest-frame forms lead to the different slopes in the r_{cv1}, r_{cv2} vs r_{rd} panels.

The distributions of r_{cv1} and r_{cv2} in Fig.5 may indicate that the different observed pulses result from the different values of r_{rd} and the different local pulse forms. What mechanism is responsible for the local pulses is not clear now. Su *et al*[36] have tentatively investigated the forming of local pulse based on a simple one-dimensional relativistic shock model. In the process of the formation of the fireball the 'central engine'[37] drives the nearby fluid (plasma) inside the fireball to generate a series of pressure waves which propagate in the form of compression wave.[38] These

waves will merge with each other to form a shock in a short time. When driving by the "central engine" ceases, which is corresponding to the onset of deceleration, the fluid near it produces an expansion wave. In this interpretation, the two kinds of waves can give birth to a local pulse: compression waves corresponding to its rise phase (acceleration time $t_{\rm ac}$) and expansion waves to its decay phase (deceleration time $t_{\rm dec}$). And thus the $r_{\rm rd}$ appearing in the paper corresponds to the ratio of $t_{\rm ac}$ to $t_{\rm dec}$ and different driving models can yield different local pulse forms (see Figs.2 and 3 in Ref.[38]).

In this interpretation, together with the knowledge of Fig.1, one can come to the conclusion that the decay timescale of the observed pulse is attributed to the resultant contributions of the acceleration timescale and deceleration timescale and the curvature timescale, while the rise timescale of the observed pulse only originates from the contributions of the two former timescales, which is similar to the conclusion in Ref.[17]. In the paper they argued that the rise timescale of the observed pulse came from the contribution of the dynamic timescale where the local pulse width was referred to as the dynamic timescale.

The light curve characteristics, a 'concave-to-convex' phase in the rise portion and a reverse phase in the decay portion, are independent of the shape of local pulse, and exist in the observed light curves of some GRBs (We find 86 source in our sample). We believe that reverse process in both portions (say, a 'convex-to-concave' curve in the rise portion and a 'concave-to-convex' curve in the decay phase) will never be detected if the radiation-emitting surface is a spherical one, no matter whether it is a spherical fireball's or a uniform jet's.

Zhang *et al*[39] have found that a structured jet has the same temporal evolutions as the uniform jet as long as the relativistic beaming angle $1/\Gamma$ is much smaller than the viewing angle $\theta_{\rm v}$. In this situation, the fireball is observed as if it was isotropic. We thus think that the characteristics of light curves in the structured jet may probably be similar to those obtained above, which deserves to be further studied.

Acknowledgment

We thank Dr Enwei Liang for his helpful suggestions.

References

[1] Marani G F, Nemiroff R J, Norris J and Bonnell J T 1997 *Astron. Astrophys. Suppl.* **190** 4311
[2] Piran T 2005 *Rev. Mod. Phys.* **76** 1143
[3] Tavani M 1996 *Astrophys. J.* **466** 768
[4] Lloyd N M, Petrosian V and Mallozzi R S 2000 *Astrophys. J.* **534** 227
[5] Baring M G and Braby M L 2004 *Astrophys. J.* **613** 460
[6] Stern B and Poutanen J 2004 *Mon. Not. Roy. Astron. Soc.* **352** L35
[7] Ghirlanda G, Celotti A and Ghisellini G 2003 *Astron. Astrophys.* **406** 879
[8] Kaneko Y, Preece R D and Briggs M S 2003 *Astron. Astrophys. Suppl.* **203** 8004
[9] Ryde F 2004 *Astrophys. J.* **614** 827
[10] Ryde F 2005 *Astrophys. J.* **625** L95
[11] Liang E W, Zhang B, Zhang B B and Dai Z G 2006 astro-ph/0606565
[12] Norris J P, Nemiroff R J, Bonnell J T, Scargle J D, Kouveliotou C, Paciesas W S, Meegan C A and Fishman G J 1996 *Astrophys. J.* **459** 393
[13] Fenimore E E, Madras C D and Nayakshin S 1996 *Astrophys. J.* **473** 998
[14] Lee A, Bloom E D and Petrosian V 2000 *Astrophys. J. Suppl. Ser.* **131** 1
[15] Lee A, Bloom E D and Petrosian V 2000 *Astrophys. J. Suppl. Ser.* **131** 21
[16] Kocevski D, Ryde F and Liang E 2003 *Astrophys. J.* **596** 389
[17] Ryde F and Petrosian V 2002 *Astrophys. J.* **578** 290
[18] Fishman G J, Meegan C A, Wilson R B, Brock M N, Horack J M, Kouveliotou C, Howard S, Paciesas W S, Briggs M S, Pendleton G N, Koshut T M, Mallozzi R S, Stollberg M and Lestrade J P 1994 *Astrophys. J. Suppl. Ser.* **92** 229
[19] Stern B and Svensson R 1996 *Astrophys. J.* **469** L109
[20] Qin Y P, Zhang Z B, Zhang F W and Cui X H 2004 *Astrophys. J.* **617** 439
[21] Shen R F, Song L M and Li Z 2005 *Mon. Not. Roy. Astron. Soc.* **362** 59S
[22] Qin Y P 2002 *Astron. Astrophys.* **396** 705
[23] Qin Y P 2003 *Astron. Astrophys.* **407** 393
[24] Qin Y P, Dong Y M and Lu R J, Zhang B B and Jia L W 2005 *Astrophys. J.* **632** 1008
[25] Jia L W and Qin Y P 2005 *Astrophys. J.* **631** L25
[26] Lu R J, Qin Y P and Yi T F 2006 *Chin. J. Astron. Astrophys.* **6** 52
[27] Zhang F W and Qin Y P 2005 *Chin. Phys.* **14** 2276
[28] Lu R J, Qin Y P, Zhang Z B and Yi T F 2006 *Mon. Not. Roy. Astron. Soc.* **367** 275
[29] Qin Y P and Lu R J 2005 *Mon. Not. Roy. Astron. Soc.* **362** 1085
[30] Band D, Matteson J, Ford L, Schaefer B, Palmer D, Teegarden B, Cline T, Briggs M, Paciesas W, Pendleton G, Fishman G, Kouveliotou C, Meegan C, Wilson R and Lestrade P 1993 *Astrophys. J.* **413** 281
[31] Schaefer B E, Teegarden B J, Fantasia S F, Palmer D, Cline T L, Matteson J L, Band D L, Ford L A, Fishman G J, Meegan C A, Wilson R B, Paciesas W S, Pendleton

G N, Briggs M S and Lestrade J P 1994 *Astrophys. J. Suppl. Ser.* **92** 285

[32] Ford L A, Band D L and Mattesou J L, Briggs M S, Pendleton G N, Preece R D, Paciesas W S, Teegarden B J, Palmer D M, Schaefer B E, Cline T L, Fishman G J, Kouveliotou C, Meegan C A, Wilson R B and Lestrade J P 1995 *Astrophys. J.* **439** 307

[33] Preece R D, Pendleton G N, Briggs M S, Mallozzi R S, Paciesas W S, Band D L, Matteson J L and Meegan C A 1998 *Astrophys. J.* **496** 849

[34] Preece R D, Briggs M S, Mallozzi R S, Pendleton G N, Paciesas W S and Band D L 2000 *Astrophys. J. Suppl. Ser.* **126** 19

[35] Kaneko Y, Preeece R D, Briggs M S, Paciesas W S, Meegan C A and Band D L 2006 *Astrophys. J. Suppl. Ser.* **166** 298

[36] Su C Y, Qin Y P, Fan J H and Han Z Y 2006 *Chin. J. Astron. Astrophys.* **6** 323

[37] Fenimore E E, Epstein R I, Ho C, lebesadel R W, Lacey C, Laros J G, Meier M, Strohmayer T, Pendleton G, Fishman G, Kouveliotou C and Meegan C 1993 *Nature* **366** 40

[38] Blandford R D and McKee C F 1976 *Phys. Fluids* **19** 1130

[39] Zhang B and Mészáros P 2002 *Astrophys. J.* **571** 876